Chapter 2

Enhancing transport in microfluidic systems

2.1 A systematic study of mixing and transport in microscale cavity flows

2.1.1 Introduction

The problem of mixing is fundamental to the miniaturization and effective operation of microfluidic circuits for biological and chemical diagnostics and analyses. Mixers, like valves and pumps, are integral components of microfluidic systems. Recently, with the increasing interest in controlling fluidic events in volumes on the order of 10^{-6} to 10^{-9} L an increasing amount of attention has been paid to the design of both passive and active mixers for microfluidic circuits. Low Reynolds numbers are characteristic of flows at the microscale (Re < 1) indicating that inertial effects are small and that the flow is dominated by viscous dissipation. Under constant pressure-driven, fully developed low shear laminar flow conditions, the velocity profile will be parabolic. Another characteristic of laminar flow is that there is very little communication between particles in different streamlines; for example, fluid in the center of the channel and fluid near the wall. In a purely laminar flow, two miscible fluids mix purely by diffusion. The Peclet number, relating convective to diffusive transport, for microfluidic systems are commonly much greater than 100, diffusive mixing is therefore slow in contrast to the axial velocity of the fluid along the channel. The penetration depth, δ, of diffusing fluid particles grows as $(D^*t)^{1/2}$ at the interface of the two fluids. For simplicity we will assume a square channel with a side length of 100 μm, flow velocities of $\sim$ 5 mm/sec, and diffusion constant $D \sim 10^{-6}$ cm^2/sec resulting in a Peclet number, Ul/D, of 105. Given that diffusion time scales across the channel are on the order of 25 seconds particles have already moved 125 mm in the axial flow direction. Clearly these time scales and distances are not compatible with microfluidic systems. A low shear laminar parabolic profile means that the average residence times of fluid particles near

the wall are much greater. Since mixing between fluids near the wall is particularly poor, clearly there are limitations on speed with which two reactants can mix in a purely laminar microfluidic environment. Besides the use of 3-D geometries, exploiting time periodic or unsteady flows is a common technique to overcome these limitations on mixing.

2.1.2 Background

Microscale flows can more or less be considered 2D, or varying only in x and y. The problem of mixing therefore becomes one of adding disturbances to perturb and therefore alter flow within the cross section of an otherwise laminar viscosity dominated 2D flow. By imposing flow components in the cross section of the flow the interface between the two mixing fluids can be increased, decreasing the distance over which diffusion occurs. Folding and stretching of the fluids to be mixed into extremely narrow striations has the advantage of maintaining the concentration gradients resulting in rapid diffusion due to the very small distances. For chaotic flows stretching and folding occurs exponentially as a function of the distance moved down the flow channel drastically reducing mixing times. These concepts have been successfully demonstrated in a variety of different micro mixers involving complex spatially varying geometries, or a series of periodically forced cross streams.

2.1.3 Principles of microscale mixing

Flows in microchannels are persistently laminar therefore the streamwise or cross-sectional velocities of particles within such flows are often negligible. Mixing commonly involves the homogenization of two initially separated fluids streams the basic idea being to maximize the interfacial area between two miscible fluids while expending the least amount of time and energy. Interfacial contact area is often increased by simple stretching and folding of the fluid. Stretching is more or less the strain on an individual fluid element. In a given flow field there may be sections where fluid elements are expanding and others where elements are contracting. In a simple shear flow this stretching occurs linearly in time. In other flows stretching may occur exponentially. Flows which display this exponential stretching have been linked to chaotic flows. A mathematical discussion of chaotic flows is given by Ottino[25].

Recently the interest in microscale mixing has prompted a reexamination of much of the literature produced on mixing theory during the 1980s and early 1990s. Many of these different theoretical constructs were proposed for enhancing mixing in 2D flows such as the blinking vortex[26] model and the pulsed source-sink model [27]. These theoretical schemes have normal spatio-temporal flow fields however have been proven mathematically to demonstrate exponential growth of fluid elements termed, chaotic advection. Chaotic advection can be seen in both 3D flows as well as unsteady 2D flows. Other constructs involve the deforming of laminated fluid streams whorls or tendrils thereby

Symbol	Parameter	Equation	Description
Re	Reynolds number	$\mathrm{Re} = \frac{\mathrm{Ud}}{\nu}$	Inertial to viscous
Sc	Schmidt number	$\mathrm{Sc} = \frac{\nu}{\mathrm{D}}$	Diffusion of momentum to diffusion of dye
Pe	Peclet number	$\mathrm{Pe} = \frac{\mathrm{Ud}}{\mathrm{D}}$	Convective to diffusive transport
Fo	Fourier number	$\mathrm{Fo} = \frac{\mathrm{LD}}{\mathrm{Ud}^2}$	Residence time of particle to diffusive time
Wo	Womersley number	$\mathrm{Wo} = \mathrm{R}\sqrt{\frac{\omega}{\nu}}$	Frequency dependent Reynolds number

Table 2.1: Shows a summary of the important dimensionless parameters for micro mixing and pulsatile micro flows.

increasing the contact area[25]. Much of this early work seems to be captured by a single kinematic concept embodied in the linked twist map (LTM) which has recently applied to micromixers[28]. The basic idea behind the LTM is that in a time or spatially varying flow streamline portraits at different instances in space and time that have crossing streamlines will generate chaotic flows. From a design or optimization standpoint the concept of crossing streamlines is the most direct and easily applied heuristic to mixing enhancement.

2.1.4 Dimensionless parameters

Dimensionless parameters such as the Reynolds number (Re), describing the relative contributions of inertial to viscous forces are another tool commonly used to understand and characterize mixing problems. Additionally, there are a number of other dimensionless parameters which are relevant convective/diffusive mixing problems such as the Peclet number (Pe), the ratio of convective to diffusive transport within the fluid and the Fourier number (Fo), the ratio of the average residence time to the diffusive mixing time. Additionally, since the aim is to study fluid mixing in the context of pulsatile flows, the Womersley (Wo) number used to describe pulsatile flows. Table 1 below summarizes the important dimensionless parameters and the properties that describe them. Here U, D, L, d, ω and υ denote the average velocity, diffusion coefficient, axial length, hydraulic diameter, frequency and kinematic viscosity respectively.

2.1.5 Micro mixers

Although it is generally difficult to classify micro mixers, they can generally be divided into two groups: passive and active mixers. Passive mixers basically rely on passive flow to reconfigure the fluid by passing it through a prescribed geometry. Active mixers rely on energy input to enhance mixing in an otherwise passively mixing flow.

2.1.5.1 Passive mixers

Passive micro mixing schemes tend to employ the lamination of parallel fluid streams or split and recombine techniques which use obstacles placed in the flow to separate and recombine lamellar fluid streams. Passive mixers can further be categorized into those that are composed of a single plane lamination and those employing three dimensional geometries. The simplest case of a passive micro mixer is the T- or Y-junction which have been used for both fluid and gas mixing. Gobby et al. studied the T mixer at a variety of inlet stream angles as well as using a throttle to stretch the mixing streams before entering the mixing chamber[29]. Other passive mixers have used hydrodynamic focusing using two perpendicular streams to squeeze the fluid into a thin jet over which diffusion occurs very rapidly[30]. In this case mixing times were reduced to a few microseconds using very high advection velocities $\sim 1 - 10$ m/s. The rapid mixing times achieved by this mixing technique have been used to study protein folding dynamics[31]. Passive mixers with obstacles have been demonstrated with mixing times on the order of 20 μs for rapid freeze quenching[32]. Optimizations of obstacle layouts for mixing in microchannels have also been performed[33].Other passive mixing systems have explored using a series of spatially varying impinging jets[34], recirculating flows (Jeon et al., 2005), in zig-zagging microchannels with interconnecting cross channels to encourage lateral transport [35, 36] or even a series of S-shaped channels to generate secondary flow circulation within the cross-section of the mixing streams.

Quite a few passive chaotic three dimensional mixers have been successfully used for effective micro mixing in several different geometries [37–41]. The staggered herringbone micro mixer[40], is a well known example that employs a spatially varying geometry of a series of angles L-shaped ridges along the bottom of the channel, referred to as herring bones, which periodically alternate direction adding asymmetry to the mixing flow. In another example a 3D square spiral towers were created within a network of microchannels[42]. Unfortunately, spatially varying geometry-based micro mixers, although effective, are difficult to fabricate, have a large amount of dead volume and require significant space with respect to microfluidic systems.

2.1.5.2 Active mixers

Active mixers use external energy to stir or agitate the flow. Many methods have been devised to mix fluids on the microscale these include: externally driven magnetic microstirrers[43], acoustic streaming [44], a flapping plates to stir the flow [45], thermocapillary flows [46], electrokinetic instabilities [47–49], dielectrophoretic [50], pulsed source-sink [51], pulsed flow [52–54], and shear superposition mixing [55]. Under the proper conditions many of these designs have been able to achieve chaotic flow.

Of the examples mentioned many of these employ oscillatory flows to enhance mixing. The

pulsed source-sink mixer of [56] embodies the theories suggested by [27], that a series of 180 out of phase combinations of time periodically forced sources and sinks could induce chaotic advection in a 2D flow. The shear superposition micro mixer (SSM)[55] is an example of a periodically forced cross-stream mixer, consisting of one main channel intersected orthogonally by a series of cross-channels. These systems are fabricated with a series of inputs to provide the periodic shear flows are successive lengths down the channel. Other studies have focused on a single unit of the SSM [57–60]. Each of these experiments has yielded chaotic advection as predicted by the LTM concept[28]. Micropumps have been used to provide a high frequency on/off switching between the two inlet channels up to 1 kHz, in effect creating a transverse layering the two fluids, where the thickness of the layer was determined by the on/off switching frequency[54]. Oscillatory mixing in a T-junction under continuous flow from both channels, as well as the effect of phase on pulsed input from the two channels have been investigated previously[52, 53]. Both studies employ micropumps to drive the oscillatory flow, however neither of these studies examines frequencies in excess of 3 Hz.

2.1.6 Formulation of the cavity problem

2.1.6.1 Large scale cavity studies

Since this work concerns a study on micro scale cavity flows therefore a brief review of cavity flows will be given. Flows within cavities are well known and often even used to gauge the validity of computational studies however in contrast there are relatively few experimental studies, especially those restricted to rectangular cavities. The most well known study of flows in cavities is probably that of Taneda[61]. Charwat categorized cavity flows into two types, open and closed, where the shear layer spans the cavity and where it reattaches at the bottom of the cavity, respectively[62, 63]. Moffat showed that an infinite sequence of vortices occur in a wedge shaped void if the angle was less than approximately146[64]. Strong oscillations in the shear layer have been observed for fixed parameters relating to the boundary layer, shear layer, free stream velocity one the cavity width exceeded a critical value[65–67]. The effect of flow oscillations on cavity drag has been investigated in a symmetric cavity on the surface of an ellipsoidal cone[68]. The basic geometry of a cavity flow is captured by 2.1. Shown are the width and height of the cavity, b and d respectively. U8 the free stream velocity and $\delta 0$ and $\theta 0$ the boundary layer thickness and momentum thickness respectively.

Here we will adopt the terminology of Gharib, 1983 in which the flow structure in cavity flows is divided into three modes for a given a fixed U8, $\delta 0$ and $\theta 0$:

1. Mode I: Is the non oscillating regime characterized by a weak, steady vortex circulating inside the cavity. Here there residence time of particles inside the cavity is expected to be very long.

2. Mode II: Once a minimum cavity width has been reached the shear layer interacts with downstream corner to create self-sustaining oscillations. Responsible for this interaction is the en-

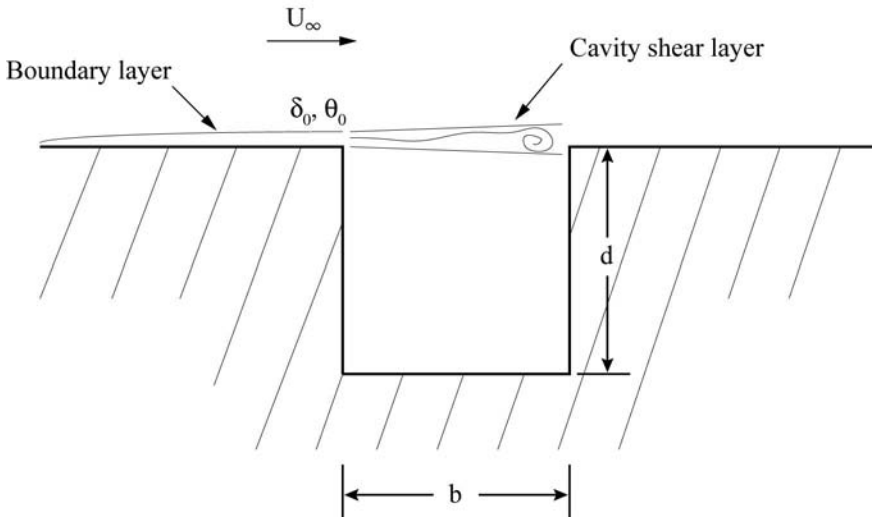

Figure 2.1: A geometric description of flow over a cavity.

trainment of fluid by the shear layer and its redirection into the cavity to replace the entrained fluid as a result of mass conservation. Under these conditions the overall phase difference between the corners of the cavity satisfied the relation $\varphi/2\pi$ = Fb/Uc= N. Where φ is the phase, F is the frequency of oscillation, b the cavity width, Uc the phase velocity of the shear layer and N the integer number of wavelengths contained by the cavity during oscillation[68].

3. Mode III: By increasing the cavity width the flow eventually transforms into wake mode where the flow reattaches at the bottom of the cavity ahead of the downstream edge. In this case the shear layer is forced to reattach at the bottom of the cavity because it can no longer sustain its entrainment. This mode is characterized by the splitting of the center vortex and the formation of two corner vortices.

2.1.6.2 Cavity flows at the microscale

Cavity flows have been studied at the microscale mainly for the manipulation of cells and other biological molecules[69–71]. However, very few measurements relating to the fluid mechanics were made. Only single particle measurements were conducted such as by optically trapping a particle and measuring its rotational velocity. From these measurements quantities such as the estimating rotational shear stress and circulation velocity were approximated. Since the focus of these studies was the manipulation of biological molecules inside of the cavity, different geometries were examined to maximize the rotationally velocities or forces experienced by the molecules within the cavity. These studies however provided no detailed results regarding the fluid mechanics of transport in and out of the cavity nor was there any examination of the parameter space under steady or pulsatile conditions.

2.2 Problem statement

Many previous studies have been able to definitively show the effectiveness of microscale mixing under pulsatile flow conditions (Dodge et al., 2003; Truesdell et al., 2003; Glasgow et al., 2004; Tabeling et al., 2004). In terms of cavity studies, elliptical cavities have been examined at the microscale however only for the purposes of manipulating cells and other biomolecules. While low Reynolds number cavity flows have been conducted on infinitely deep cavities, no parametric investigation exists on microscale cavity flows which focus on the fluid mechanics of the cavity with out-of-plane boundary layers, a situation more relevant to real world flows. Similarly, there is no investigation of pulsatile flows in microscale cavities.

Microscale cavities were therefore investigated to determine how the frequency and amplitude conditions of the flow field affect the ventilation or mixing of the cavity contents with the freestream. The homogenization of two intially separtated fluids will be adopted as a general definition of mixing. However this study seeks to examine the mixing of two intially separated fluids, one in the freestream and one in the cavity, not to directly to examine mixing inside the cavity region. The goal is to understand how to better mix the ventilated cavity contents with the freestream aside from the situation observed in steady, purely laminar flow where contents advected out of the cavity remain near the wall.

To overcome the geometrical complexities of many of the microfluidic mixers a simple rectangular cavity was chosen for the purposes of the study. Although the aforementioned studies do exist in which some comparisons can be made, in terms of the fluid mechanics and microfluidic fabrication, elliptical cavities are difficult to parameterize namely due to the definition of their intersection with the freestream and the ability to resolve this boundary accurately with current microfabrication techniques, and the huge impact this has on flow separation, making case by case comparisons difficult.

In addition these experiments sought to develop techniques to control cavity ventilation purely through the manipulation of the flow field. To accomplish this study the following three objectives were set:

1. To understand the relationship between ventilation and Reynolds number and cavity geometry under steady flow conditions steady.

2. To investigate the affect of pulsation frequency on the ventilation properties of the cavity.

3. To determine the relevance of pulsation amplitude on cavity ventilation.

Besides the problem of mixing in Lab-on-Chip microfluidics, there are many real world examples where this form of analysis is particularly useful. For example, the elution of a drug and subsequent mixing of the drug with the fluid of interest such as blood. What is the most effective means of

distributing a substance throughout the main body of the flow in order to distribute the drug evenly to the target tissues? Unsteady cavity flows also have analogs in other biofluids flows such as in the junctions of grafts and stents or the alveolus of the lungs. Take the latter case for example, in the alveolus of lung, ventilation of gas into or out of microenvironment, and the degree of mixing or ventilation of alveolus is important to maintaining blood oxygen levels. This investigation also holds merit in the search for effective strategies to control transport in microfluidic systems in that many of the current mechanisms for pumping fluid at the microscale are inherently pulsatile in nature.

2.2.1 Approach

The systematic study of microscale cavities requires the ability to provide high frequency large amplitude oscillation onto a mean flow as well as methods to acquire information about the flow fields. PIV remains the most widely used measurement technique for acquiring velocity fields of microflows due to its ability to be implemented optically without disturbing the flow and its versatility in terms of its application. Accurate measurements of the cavity flow fields are crucial to predicting particle trajectories for the residence time calculations which will be used to estimate the ventilation properties of the flow conditions. These PIV measurements will also be used to feed Finite Time Lyapunov exponent calculations to aid in identifying flow boundaries explaining the ventilation and mixing behavior.

2.3 Description of the experimental setup

The goal of the experimental setup was to provide a known high frequency oscillation with a fixed mean flow into microfluidic chip which could be imaged in an inverted microscope. Since push pull syringe pumps are limited to around 10 Hz, high frequency, large amplitude oscillatory flow will be provided by a voice coil (Brel and Kjr, 4810 mini-shaker) used to pinch an elastic tube downstream of a syringe pump (Harvard Apparatus, Holliston, MA.) providing a mean flow. A fluidic capacitor will be installed between the syringe pump and the elastic tube to damp out any fluctuations created by the operation of the pump. The inner diameter of the elastic tube is 2 mm with a 780 μm wall. The voice coil probe has a diameter of 2.4 mm resulting in a displacement volume of approximately 8 μL. Data is acquired using a National Instruments data acquisition card and the motion of the probe is controlled in open loop by using a Matlab script which provides 2 mm displacements of the probe up to 150 Hz. Microscale flows will be observed using an Olympus IX-70 inverted microscope. Image acquisition will be performed using an Imperx Lynx. Flows will be illuminated using a 200 mJ Nd:YAG New Wave Gemini lasers allowing for a 15 Hz double exposure repetition time and phase averaged reconstruction of high velocity flows. A schematic of the experimental system is shown in Figure 2.2. A diagram of the relevant cavity geometry can be seen in Figure 2.2.

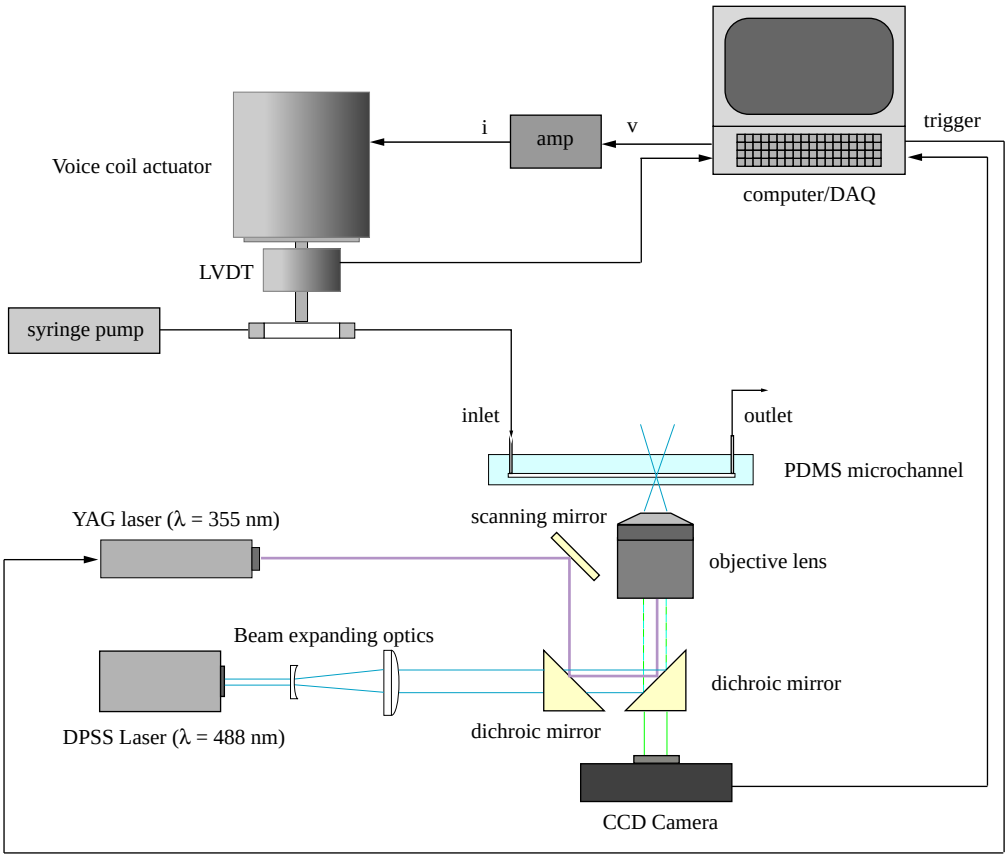

Figure 2.2: A diagram of the experimental setup to be used for the microscale cavity flow studies. The voice coil and LVDT will be used to provide precise frequency and flow velocity amplitude inputs over the steady flow provided by the syringe pump.

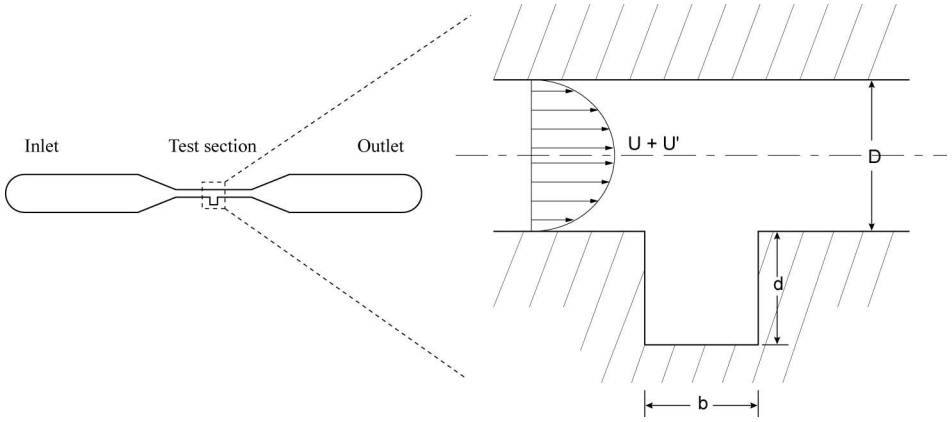

Figure 2.3: Shows the geometry of the microscale cavity including the width and depth of the cavity, b and d respectively as well as the width of the main channel, D. The height of the cavity in the out of plane dimension was fixed at 100 μm. Also shown are the relevant fluid parameters U and U'.

2.3.1 Optical setup

To clean up the laser pulse from the Nd:YAG the laser light was first passed though a weak spatial filter with an optical pinhole of size of 50 μm. The beam was then expanded and passed through a 5° holographic diffuser. The diffuser has the function of evening out any regions of unusually high energy density left in the beam producing a close to Gaussian output. Flows were imaged using a 100x oil immersion apochromatic lens from Olympus. In order to condense the image onto the camera CCD, a 0.63 x tube coupler was used to couple the image to a Imperx Lynx. The camera and lasers were triggered using a National Instruments PCI-6602 timing card.

2.3.2 Microfluidic chip design

The microfluidic channels were designed to contain single cavities such that there was no cross talk between structures in the flow. To minimize any 3-dimensionality to the flow the microchannel was fabricated to a depth of 30 μm. Since the flow enters through a vertical inlet and outlet and is pulsatile flow first enters a larger section of the microchannel with a 750 μm width before tapering to 50 μm in the test section containing the cavity. The length of the flow channel after the cavity is 2 mm to ensure that any potential instabilities remaining in the flow from the inlet and outlet, producing an even laminar flow over the surface of the cavity.

The microfluidic chip was fabricated through well documented methods of soft lithography. SU8-25 Photoresist was applied to a Si wafer to produce a thickness of 30 μm and exposed to the cavity pattern using a 20000 dpi photomask. Once the mold was developed, a two part RTV 617B was poured over the mold and baked in the oven at 80°C to cure the polymer. The PDMS chip was then sealed to a glass cover slip using O_2 Plasma treatment to ensure adequate bonding.

Large scale fluid mechanics studies have the benefit of relative size with regards to having sharp edges and minimal surface roughness. These attributes cannot always be taken for granted with work at the microscale. Since this study is concerned with the fluid mechanics of cavity flows the mold was measured using SEM measurements to confirm the channel height was well as examine the relative smoothness of the mold. A representative SEM image of the bottom of a 50 μm wide cavity can be seen in Figure 2.4.

2.3.3 Micro Particle Image Velocimetry

Micro PIV studies yield velocity fields of particles moving within the flow. The methodology for applying DPIV to microchannel flows is well established [72, 73]. Results from μPIV experiments on micro cavities were used to quantify values such as the mean and oscillatory velocity components and channel profiles as well as analyze properties such as shear stress within the cavity. Much of the complexity in imaging microscale cavity flows comes from the huge velocity gradient spanning

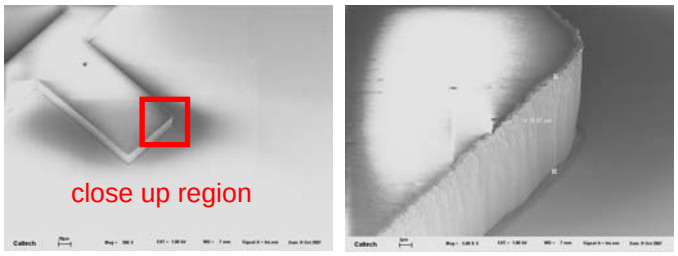

Figure 2.4: An SEM of the cavity. On the left is a zoomed out view showing the region given for the close up. On the right is the side profile of the cavity. The image is taken at a 30 viewing angle so the sine of the view angle makes the actual mold height 31.1 μm.

the freestream to the base of the cavity. Complete reconstruction of the velocity field within a microscale cavity depending on the freestream velocity and cavity geometry can involve performing μPIV measurements with time increments spanning 4 orders of magnitude. PIVview a PIV analysis package was used to mask the PIV frames isolating areas of common velocity within the cavity as well as process contained in them. The velocity fields from the μPIV experiments were then applied to particle tracking schemes to identify the residence times of the particles and quantify the time averaged Lyapunov exponents of particle trajectories within the flow.

2.3.4 Analysis of microscale transport

2.3.4.1 Definition of Particle Residence time

PIV velocity fields were used to provide particle tracking trajectories in order to compute the residence time of particle, or the time the particle remains within the cavity for different flow input conditions. The following equation was used to calculate the particle residence time:

$$T_R = \sum_i \frac{|x_i - x_{i-1}|}{|v_i|}; x_i \in X \tag{2.1}$$

where x and v are the displacement and velocity vectors for each particle, respectively. TR represents particle residence time, i denotes the number of time steps that the particle is still in the area of interest, and X the region of interest. Residence times will be used as a tool to examine the ventilation or mixing process between the cavity and free stream.

The residence time code was written in Matlab. Particle velocities were determined by a weighted average based on the particles distance to the nearest 16 surrounding grid points. Time series for the steady cases were reconstructed by replaying time averaged steady velocity over and over again into the residence time simulator. Steady cases analyzed the residence times of 5000 particles seeded randomly in the lower half of the cavity. Each particle was tracked for a total of 10000 time steps. If a particle did not exit the cavity within the allotted 10000 time increments the residence time was flagged as infinite.

Phase averaged velocity data was taken to collect 10 phase increments of each at pulsatile flow frequency examined Pulsatile flow cases examine random distributions of only 1000 particles however they were tracked over 50000 time steps. The reason for this is the small phase increment of subsequent velocity fields in the time series.

2.3.4.2 Lagrangian Coherent Structures

Lagrangian Coherent Structures (LCS) was used to identify separatrices within the flow that form boundaries to transport in order to visualize structures present in the microscale cavity which may affect the ventilation process. The Lyapunov Exponent is an average measure of the exponential rate of divergence of the trajectories of two closely located particles within the flow field. LCS are the local maxima of the FTLE field and refer to the manifolds that exist as parts of hyperbolic structures within the phase space of the flow (Shadden et al., 2005).

Velocity information from the μPIV data was processed using MANGEN to produce the FTLE fields. MANGEN is publicly available software created by Francois Lekien and Chad Coulliette. Steady flows were processed by replaying a single time averaged steady PIV repeatedly for a given time period. The steady data was processed using 60 frames with a time step of 0.0714 seconds for a total of 4.28 seconds. The integration time was adjusted according to the freestream flow rate to prevent a large number of particles from exiting the FTLE region during integration. Pulsatile flows were processed using 100 phase slices per cycle over a time frame of 2.5 periods.

This form of analysis was able to elucidate key flow features which affect the transport properties of microscale cavities as well as aid in the identification of areas of flow separation, and stagnation that exist on different timescales. In the case of the pulsatile flows LCS proved particularly useful to in revealing the instantaneous boundaries in the rapidly changing flow field and how their evolution through time influences mixing between the cavity and freestream.

2.4 Experimental results

2.4.1 Steady flow in microscale cavities

An investigation into steady flows microscale cavities was performed to determine the dominant modes of transport under steady flow conditions. These studies were also useful in identifying separations and the onset of circulation in the cavity under steady flow conditions for varying cavity geometries. The investigation into steady flows also provides us a starting point for interpreting the pulsatile flow results presented in the Section 2.4.2. A compilation of all residual plots for all steady cases examined can be found in Appendix E.

Three cavity aspect ratios were examined 0.5, 1, and 2 spanning Reynolds numbers 0.1 – 100.

Aspect Ratio	Freestream Reynolds Number								
0.5	0.1	1	10	15	16.7	20	30	50	100
1	0.1	1	10	20	22.2	23.3	24.4	30	50
2	0.1	1	10	20	30	40	50	75	100

Table 2.2: A summary of the various cavity flow configurations investigated under steady flow.

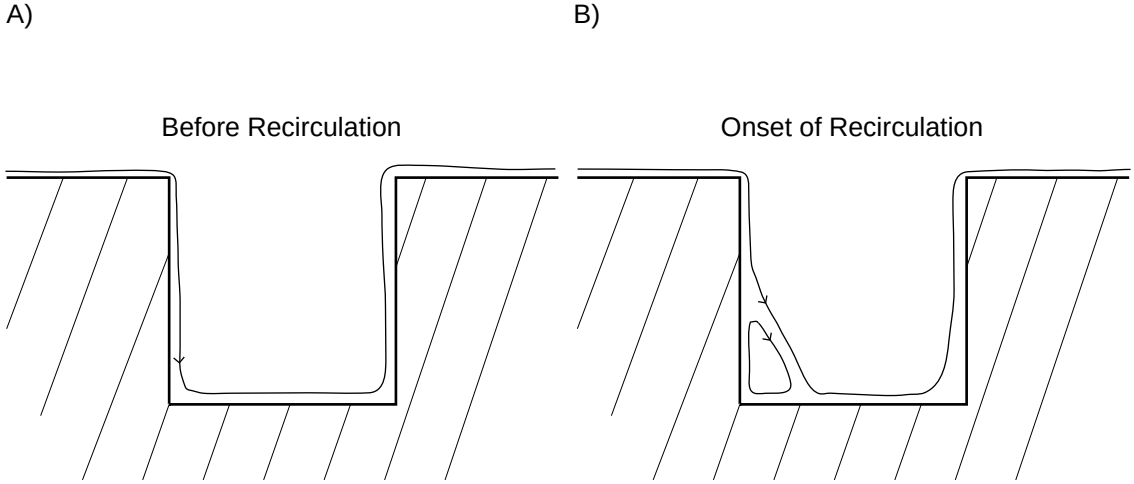

Figure 2.5: A schematic representation of the onset of recirculation in the microscale cavity under steady flow conditions. A) Shows flow before the onset. B) Show flow after the onset of recirculation.

A summary of the particular flow rates examined for every cavity case is presented in Table 2.4.1. Particular attention was paid to capture the transition region to separated flow.

2.4.1.1 Separation and reattachment versus Re and geometry

For Reynolds numbers less than 10 there is no separation for cavites of any of the aspect ratios examined. The relatively low Reynolds number of the flows examined combined with the similarity in dimensions between the freestream channel depth and the boundary layer thickness, results in a very diffuse separation compared to that normally observed or simulated in cavity flows. Careful attention was paid to capture the onset of circulation for cavity aspect ratio 0.5, 1 and 2 the onset of recirculation occurred at Reynolds number 16.7, 23.3 and 40 respectively. The onset of recirculation is defined schematically in Figure 2.5. A plot of these two parameters can be found in Figure 2.6. A rough fit of onset of recirculation versus Reynolds number shows a linear trend, however such a relationship is probably the result of the number of points and not an existing physical trend in the data. Streamline images generated from PIV velocity fields enabled the visualization of the separation and reattachment regions along the boundaries of the cavity. Typically for aspect ratio 1 and 2 cavities at the onset of recirculation the separation has a triangular form, separating from the leading edge of the cavity and reattaching to the cavity base. As the freestream Reynolds number

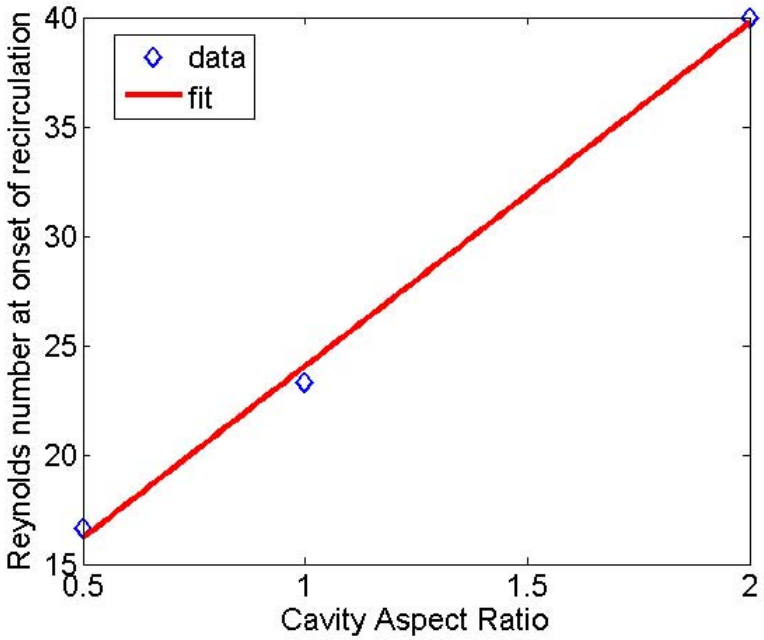

Figure 2.6: A plot of the onset of recirculation versus cavity aspect ratio revealing the linear relationship between the two parameters.

is increases first the location of separation and the reattachment expand moves along the base of the cavity until reattaching on the trailing edge wall. Upon reattaching to the trailing edge the separation does not immediately jump to the trailing edge. At this state the morphology of the recirculation maintains its oblong character until the freestream velocity is increased sufficiently to reattach the separation on the trailing edge. The position of the reattachment away from the leading edge cavity wall was measured for cavity aspect ratios 1 and 2. The plot of this behavior is shown in Figure 2.7. The relative stability of the separation is visible in the rate at which the curves in Figure 2.7 reach full separation or 1. The steeper rise indicates that the shorter width of cavity aspect ratio 1 versus 2 makes the separation in this case more stable. Aspect ratio 0.5 was not examined due to the depth of the cavity the separation is stable and always located on the trailing cavity edge wall.

2.4.1.2 Shear layer penetration depth and the affect of freestream Reynolds number

Another affect examined at the microscale, especially predominant at lower Reynold numbers in the range was the apparent diffusion or broadening of the shear layer over wide region relative to the cavity. The recession depth is represented schematically in Figure 2.8 and the data is shown in Figure 2.9. When examined closer it can be seen that in these cases the separation point is actually located at a position along the height of the leading edge wall. Due to the relative simarlity in dimensions between most fluid geometries in the flow the microscale cavity is more resistant to separation due to the presence of the opposing wall. On the other end of the spectrum towards higher Reynolds

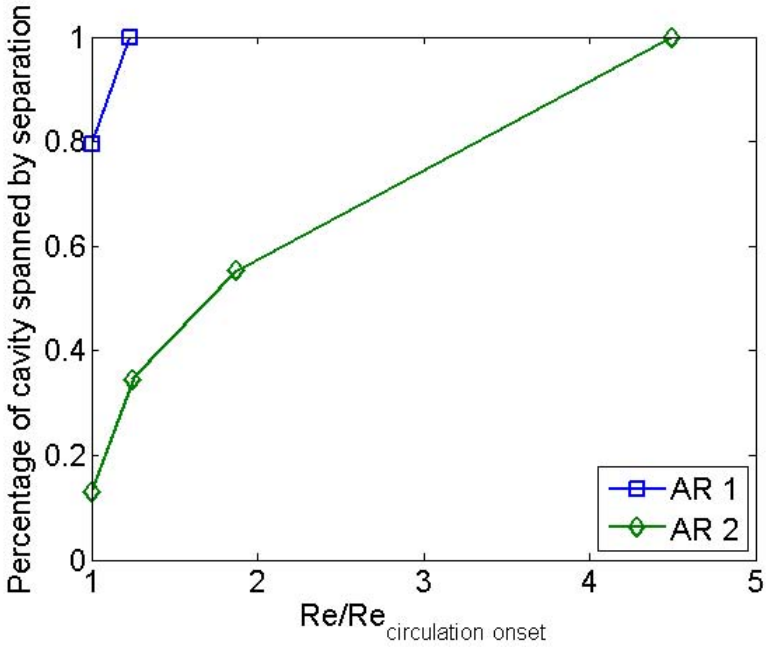

Figure 2.7: Displays the percentage of the cavity spanned by the reattachment for AR = 1 and 2.

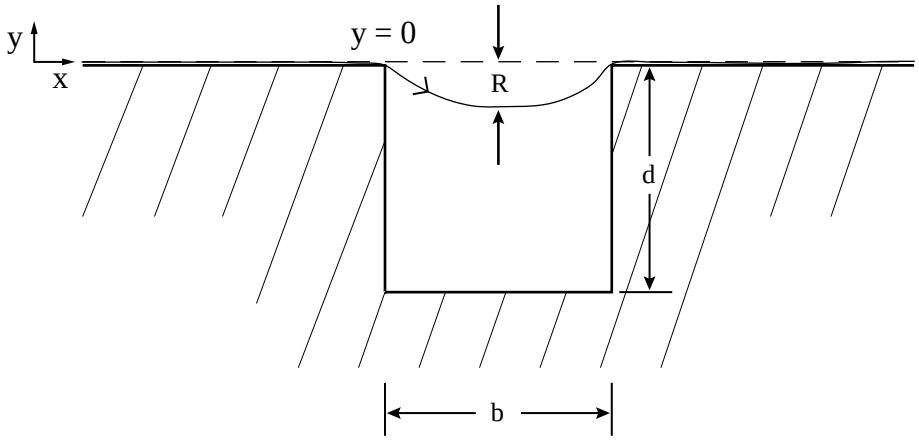

Figure 2.8: A schematic representation of the cavity recession depth, R. The y = 0 line is taken as the top of the cavity.

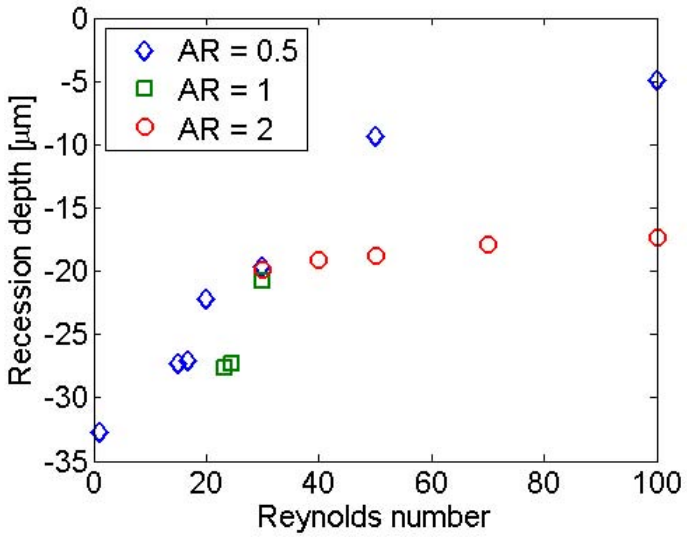

Figure 2.9: The recession depth of the shear layer versus Reynolds number for steady cavity flows.

numbers, we see the affect of fluid entrainment into the shear layer in that much higher Reynolds numbers are required for the higher aspect ratio cavities to minimize the penetration depth to the top of the cavity. For example rise of the aspect ratio 0.5 much more rapidly approaches the cavity top located at 0 μm. Whereas at Re = 100, the maximum Reynolds number examined, the penetration depth in the aspect ratio 0.5 cavity equals 4.9 μm, the penetration depth of the shear layer in the aspect ratio 2 cavity is 17.3 μm.

2.4.1.3 Tangential circulation velocity and freestream Reynolds number

The tangential circulation velocity was examined for the full range of Reynolds numbers and cavity aspect ratios after the onset of recirculation in the cavity in order to attain an estimate for the circulation in the cavity. Since establishing a precise boundary for the recirculation was difficult circulation was not directly measured. Examining the plot shown in Figure 2.10, initially the circulation velocity increases slowly. Towards higher Reynolds numbers in excess of the curve continues to climb in an almost linear fashion. This effect seems representative of the isolation from the freestream velocity provided by the cavity depth and related to the broadness of the shear layer. As the free stream velocity increases the circulation grows in size and moves toward the top of the cavity until it reaches a minimum bounded by the streamlines of the freestream. One of the relationships established by the studies of Shelby et al. was a linear relationship between radial acceleration and rotational frequency of a particle trapped in the cavity circulation to volumetric flow rate. In this study, the completely linear trend is most likely the result of the fact that over the range of Reynolds numbers in their study the circulation is already located at the cavity top and hence responsed linearly to linear increases in freestream flow rate.

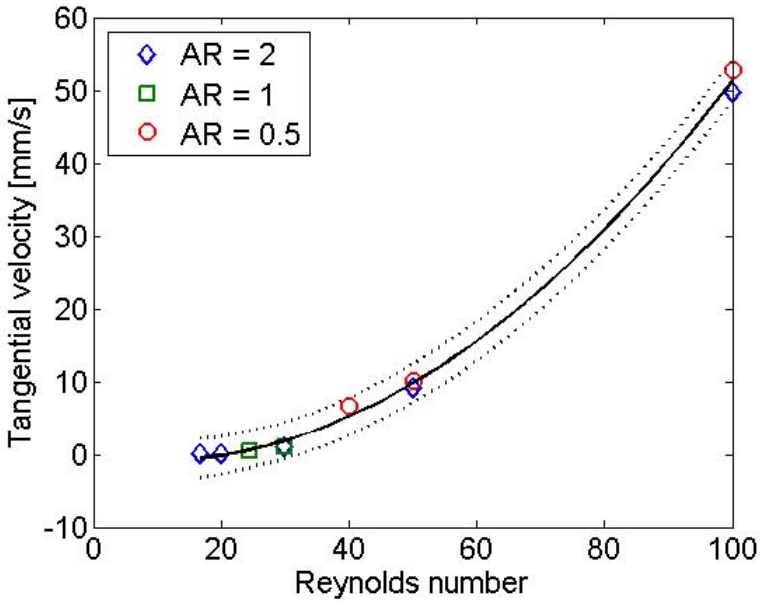

Figure 2.10: A plot of the tangential velocity of the circulation versus Reynolds number. The dashed lines show the 95 % confidence interval for the data.

2.4.1.4 The influence of Reynolds number and geometry on shear stress across the top of the cavity

The affect of increasing Reynolds number showed that the shear across the top of the cavity increases linearly with Reynolds number. The top of the cavity is defined as the y = 0 line represented in Figure 2.8. Plotting the points seems to indicate that independent of aspect ratio all points seem to collapse onto a single line, meaning that shear at the top of the cavity is independent of the cavity aspect ratio as well as the location of the recirculation. Figure 2.11 shows a scatter plot of average shear values across the top for various cavity experiments as well as a linear fit. The dashed lines above and below the linear fit represent a 95% confidence interval, showing fairly good agreement between measurements. Additionally, in light of the tangential velocity data, circulation velocity is not a linear function of the shear stress for Reynolds numbers less than 100. It however remains to be determined whether this relationship becomes linear at Reynolds number in excess of 100.

2.4.1.5 Residence times of steady cavity flows

The average velocity fields were used to compute the average residence times of particles seeded inside the bottom half of the cavity region. Two flow regions are present in the cavity and their relative size affects the number of instances in the distribution as well as varies the number of peaks from 1 to 2. These two regions are represented in Figure 2.12. The first peak represens particles seeded in a region outside or near the boundary of the separation where the streamlines from the

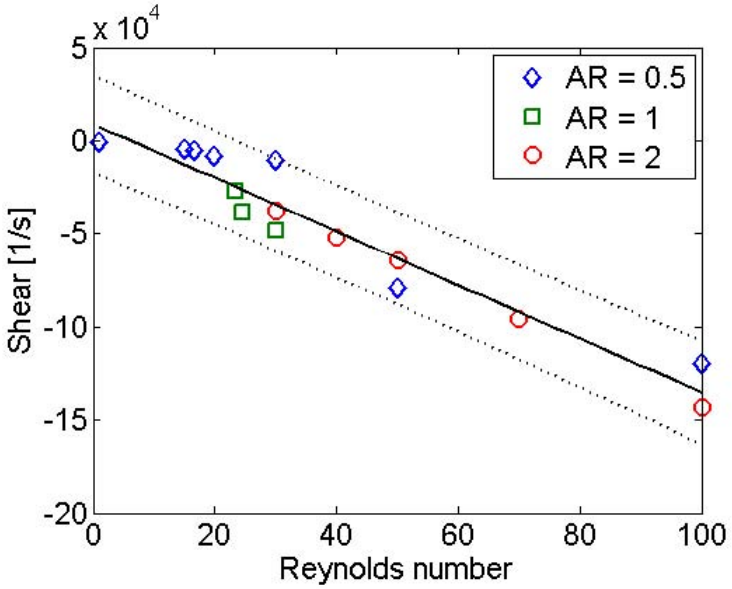

Figure 2.11: A plot of the average shear stress at the top of the cavity versus Reynolds number for cavity AR = 0.5, 1, 2.

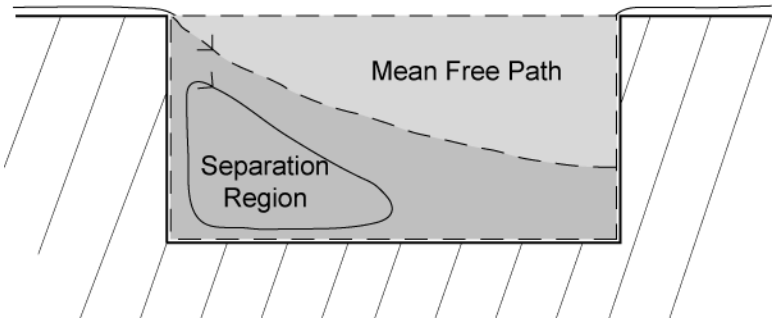

Figure 2.12: A schematic of the two regions representing the individual peaks in the residence time plots. The first peak correlated to particles in the mean free path. The second to particles in the recirculation region.

Aspect Ratio	Freestream Reynolds number					
0.5	1	15	16.7	20	30	100
1	23.3	24.4	30			
2	40	50	75	100		

Table 2.3: Summarizes the residence time calculations performed under steady flow conditions.

freestream enable them to quickly find a path to the main part of the flow, referred to as the mean free path back to the freestream. The second, for particles seeded inside the separation region. Particles here can do one of two things, escape or remain trapped infinitely in the circulation or a region of stagnation near the boundaries of the cavity.

The residence time plots show the affect of the growing size and strength of this circulation region by the appearance of the second peak, a growth in its relative size to the mean time of flight path and lastly by a decrease in the number of instances in the histogram, representing the fraction of particles that were not infinitely trapped inside the separation. These affects are illustrated in Figure 2.13 through Figure 2.14. These regions individually are also representative of the two extremes of the cavity flows. At Reynolds numbers where there is no separation present particles are advected with the streamlines out of the cavity producing a mean time of flight path peak. At very high Reynolds numbers the circulation fills the entire width or height of the cavity depending on its limiting dimension as a result of its aspect ratio, trapping all particles inside. Table 2.4.1.5 summarizes the steady flow conditions for which residence times were calculated.

The residence times were normalized by a timescale assigned by dividing the cavity width by the freestream velocity. When plotted on a log scale versus the freestream Reynolds number the residence time calculations produced the plot in Figure 2.15. Figure 2.15 shows the presence of peak in the normalized residence time right before the onset of recirculation. In this range the fluid goes through a transition. At Reynolds numbers far below the transition the flow the boundary layer of the freestream is able make the corner and adhere the base of the cavity. In this case nearly all the particles escape from the cavity. As the flow accelerates, the velocity gradient from the top to the bottom of the increases meaning residence times change only slightly while the velocity of the freestream increases significantly producing an increase in the normalized residence time. This can be seen in the transition from Re = 1, to Re = 27 in the AR = 0.5 case. These Reynolds numbers are equivalent to flow rates of 1.8 μL/min and 27 μL/min. Here the flow rate increases by a factor of 10 but the residence times only increase by a factor of 2 or so, indicating the growth of a stagnation region. Right before the onset of circulation the normalized residence times reach a maximum before dropping as the circulation begins. Somewhere past this point the residence time reaches a minimum where the circulation is strong enough to introduce particles in the base of the cavity to the freestream flow but not trap them. As the strength of the recirculation increases the result on the residence time has two affects: first the number of particles in the distribution drop significantly

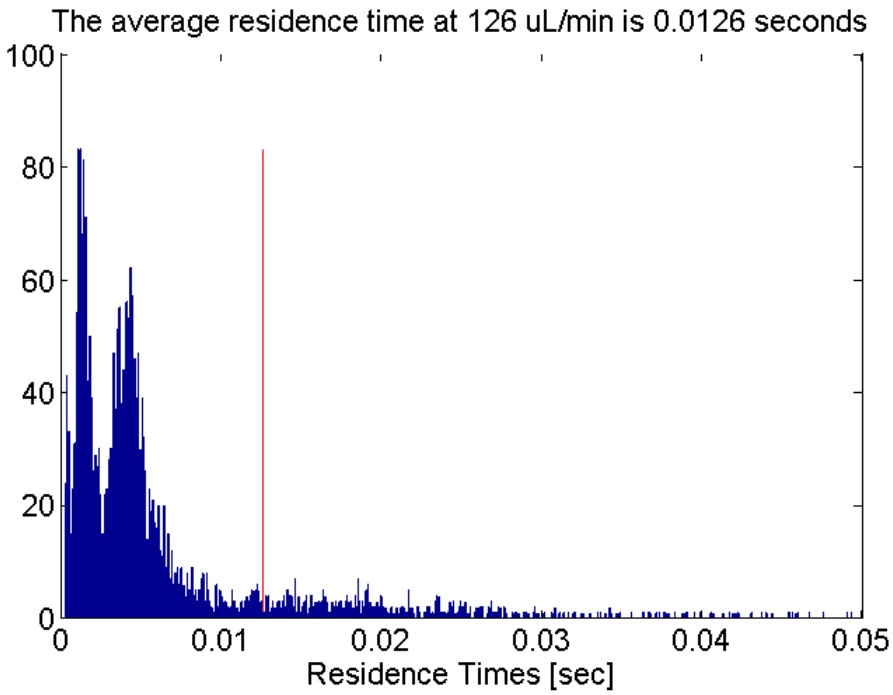

Figure 2.13: The residence time distribution for the AR 2 cavity at 126 μL/min or a Re of 75. The two peaks representing the mean free path and the escape route through the recirulation. The relative size of the peaks represents the relative size of the recirculation region versus the mean free path region. The average residence time in this case is 0.0126 seconds.

representing the fact that very few particles are located in a position where their trajectory presents a path to the freestream, if it does they exit very quickly, and second if the particle does not begin on one of these trajectories the tendency is for particles to be trapped indefinitely in the recirculation. It is difficult to interpret the residence time plot without prior knowledge of the flow occurring in the cavity therefore the residence time distributions are presented in Appendix E. For example, residence time calculations such as at AR = 0.5, Re = 100 produced an infinite residence time and therefore are not represented on the plot. The residence times indicate that in terms of timescale the best cavity ventilation occur at very low Reynolds numbers where no separation is present as well as right past the onset of recirculation where the weak circulation is able to move particles in the base of the cavity on trajectories where they can be entrained by the free stream flow. Since a purely laminar flow has the affect of poor communication between particles in different streamlines it suggests that the second minimum right past the onset of recirculation is best in terms of the mixing and ventilation of the cavity under steady flow conditions.

2.4.1.6 Lagrangian Coherent Structures in steady cavity flows

For the steady flow cases the FTLE fields displayed the presence of the separation, reattachment as well as the trapping region formed by the circulation region. Although Lagrangian Coherent

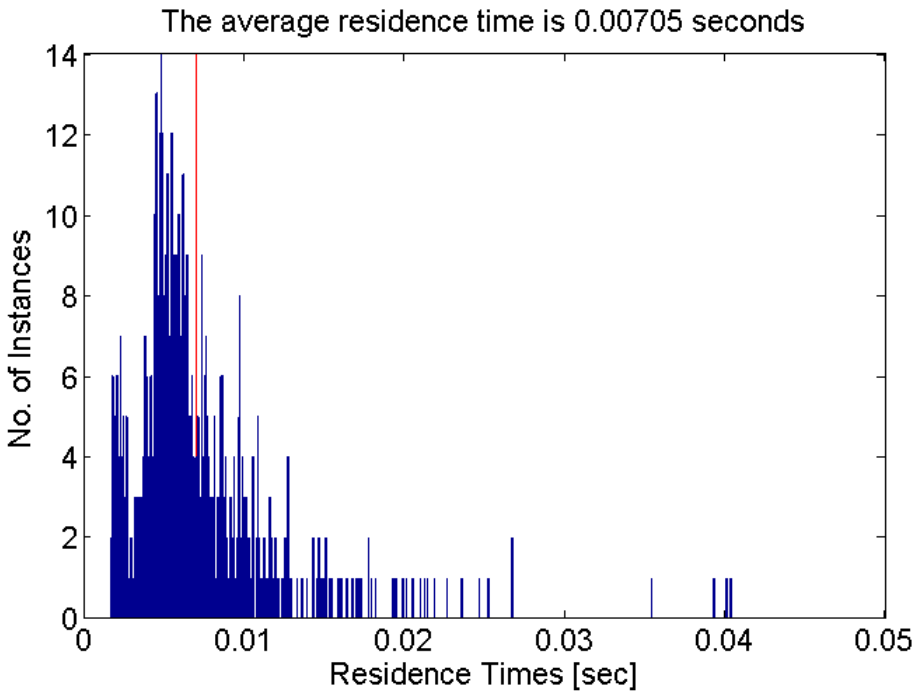

Figure 2.14: The residence time distribution for the AR 2 cavity at 180 μL/min or a Re of 100. The two peaks representing the mean free path and the escape route through the recirulation. The relative size of the peaks represents the relative size of the recirculation region versus the mean free path region. The average residence time in this case is 0.007 seconds.

Structures were applied for the visualization of the flow structures in all steady cases, for the purpose of this discussion the LCS at 180 μL/min or Re = 100 will be examined. At Re = 100 the forward time LCS clearly reveals the reattachment on the trailing edge of the cavity wall as well as an repelling LCS related to a stagnation region in the lower right corner of the cavity. The reattachment is more easily visualized by examining the full FTLE field in Figure E.20. The corresponding backward time FTLE field in Figure E.19 reveals the presence of the separation towards the upper extent of the leading edge wall. The overlay of the backward time and forward time FTLE fields can be viewed in Figure 2.16. The overlay was produced by masking all but the highest values in the FTLE field for both the forward time and backward time calculations. The colormap on the forward time FTLE field was then flipped in order to distinguish between attracting and repelling LCS. In the LCS overlay in Figure 2.16 the backward time LCS are colored pink and the forward time structures are colored to the blue end of the colormap. The overlay allows the visualization of the trapping region formed by the attracting and repelling LCS within the cavity. Also apparent from the overlay is the difficulty particles have in leaving the recirculation region due to the transport boundary formed by repelling LCS surrounding the recirculation region.

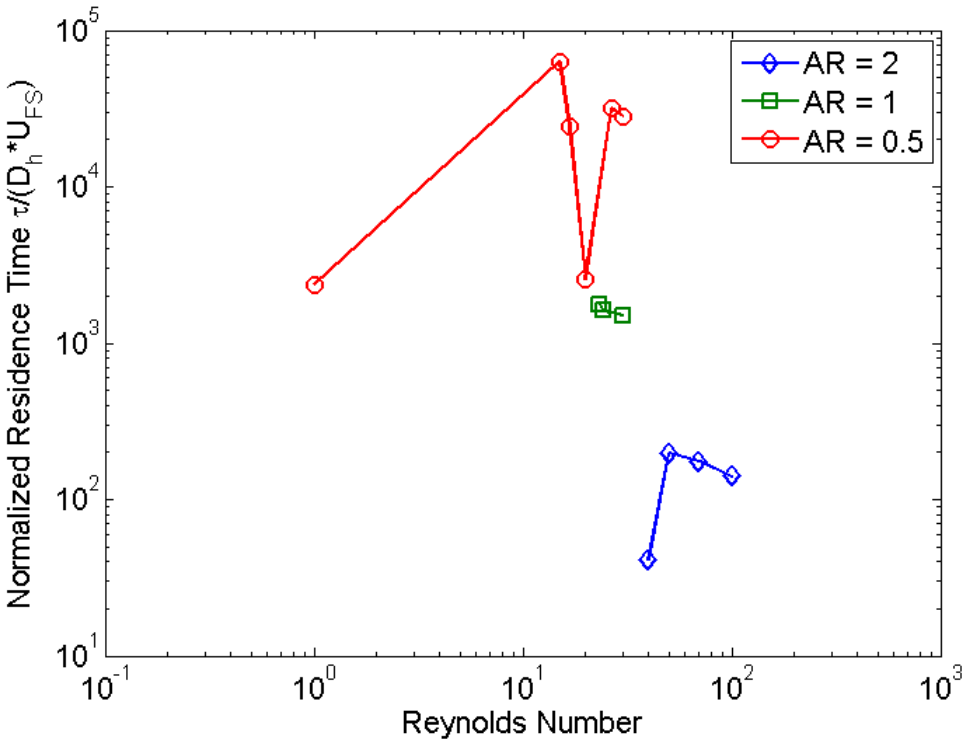

Figure 2.15: A log plot of the normalized residence times versus Reynolds number for cavity AR = 0.5, 1, 2. Residence times are normalized by the cavity with divided by the freestream velocity.

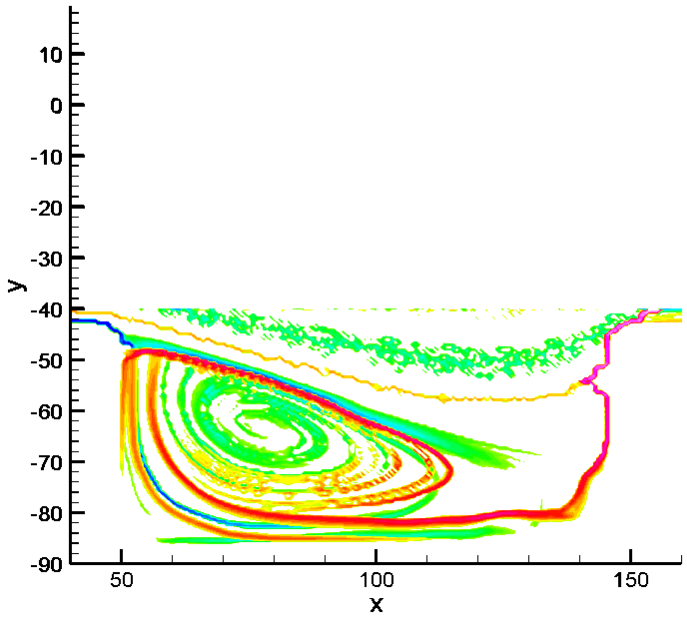

Figure 2.16: Shows the FTLE field at AR = 2 and a flow rate of 180 μL/min.

2.4.1.7 Dimensionality of microscale flows - affect of out-of-plane dimension 30 μm and 100 μm.

One of the benefits of this study is it allows us to comment on the affect limited channel depth and its influence on cavity circulation. Compared to previous microscale cavity studies conducted at 100 μm cavity depth, the transition to circulation occurred much earlier. In this instance we see a reduction from 16.7 to approximately 1 for an out-of-plane depth of 30 μm and 100 μm respectively. These results are further confirmed by the results of Shelby and Chiu where in order to get increased cavity rotational frequency they move from a channel depth of 30 microns to a channel depth of 50 μm. This increase in cyclical frequency is in response to a decrease in length of the out-of-plane boundary layer.

2.4.1.8 Dimensionality of microscale flows - affect of out-of-plane dimension 30 μm and 100 μm.

One of the benefits of this study is it allows us to comment on the affect limited channel depth and its influence on cavity circulation. Compared to previous microscale cavity studies conducted at 100 μm cavity depth, the transition to circulation occurred much earlier. In this instance we see a reduction from 16.7 to approximately 1 for an out-of-plane depth of 30 μm and 100 μm respectively. These results are further confirmed by the results of Shelby and Chiu where in order to get increased cavity rotational frequency they move from a channel depth of 30 microns to a channel depth of 50 μm. This increase in cyclical frequency is in response to a decrease in length of the out-of-plane boundary layer.

2.4.1.9 Shape of z-profile

The objective lens of the microscope due to is thin focal depth allows us to examine the shape of the out-of-plane boundary layer by imaging through the depth of the cavity and the freestream. Cavity flows were imaged for a cavity AR = 1 for flow rates of 1.8 μL/min and 54 μL/min or Re = 1 and 30 respectively. Seven slices of the cavity were imaged to reconstruct the flow. The first velocity profile slice was taken approximately 500 nm off the channel base, another at 1.5 μm off the channel base and the rest in 4 μm increments until 22.5 μm into the cavity depth. The complete z-profile was not acquirable due to the presence of out focus particles limiting the depth that could be images. Figure 2.17 shows the reconstruction of the 2D slices for the entire AR = 1 cavity at Re = 1. The entire cavity at Re = 30 was not plottable due to the large gradient in the velocities from the top of the cavity to the bottom and the limitations of the vector scaling properties of the 3D vectorfield plotter in Matlab. Figure 2.18 shows a reconstruction of the u-velocity profile in the x-z plane. The profile as expected is parabolic, the same as in the x-y plane. The peak velcocity is 2 times the mean

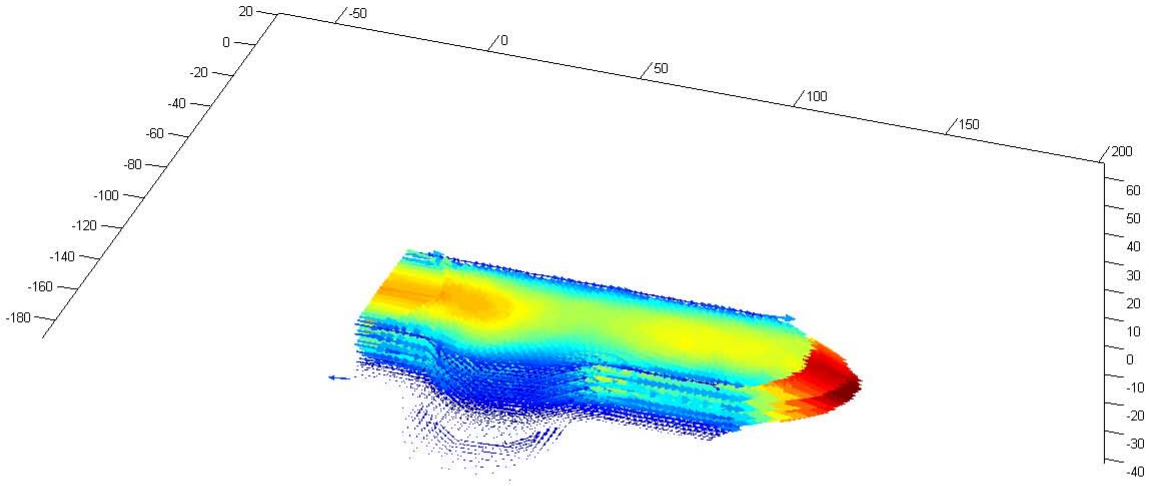

Figure 2.17: A reconstruction of the 3D flow profile of the cavity at 1.8 μL/min or Re= 1.

of 20 mm/s, exactly what is predicted by Pouseille flow.

2.4.2 Enhancing transport through pulsatile flow

Pulsatile flows were examined to determine the affect of unsteadiness on transport out of microscale cavities. For this investigation 4 frequencies, 13 Hz, 64 Hz, 80 Hz, and 113.1 Hz were examined for a mean flow of 1.8 μL/min in the AR = 0.5 cavity. These frequencies correspond to Wo numbers of 0.33, 0.75, 0.84, and 1. Here the Womersley number is defined slightly differently for cavity flows than for channel flows. The modified Womersley number used in this study was defined as,

$$\mathrm{Wo} = \mathrm{D_h}\sqrt{\frac{\omega}{\upsilon}} \tag{2.2}$$

where Dh is the hydraulic diameter of the cavity top, ω is the frequency in rad/s and ν the kinematic viscosity. The affect of amplitudes was also examined at 113.1 Hz at two voice displacements 0.4 mm and 0.2 mm corresponding to flow peak to peak amplitudes of 80 mm/s and roughly 5 mm/s respectively. It is readily obvious that is ratio is not equivalent indicating that the response is not linear. The reason for this is the experiments were started at 0.4 mm, which provided 80 mm/s peak to peak amplitude. The assumption prior to what is indicated by the data was that this response should proceed linearly given the incompressibility of the fluid. The peak to peak amplitude did not remain constant in the case of the pulsatile cases at 0.4 mm amplitude either. Possibly this affect

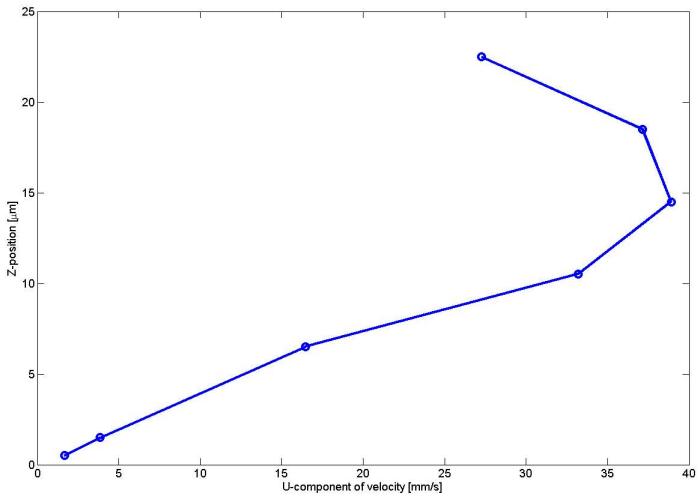

Figure 2.18: A plot of the z-profile in the cavity freestream at 1.8 μL/min or Re = 1. The peak u-velocity is roughly twice the mean of 20 mm/s, as predicted by Pouseille flow.

was due to some phase lag in the response of the tube to high frequency excitation in addition to the fact that there are most likely unknown system dynamics associated with the transfer of that pulsation to the cavity flow area through the many couplings required to connect to cavity flow channel.

Reconstructing velocity fields for the pulsatile cases was particularly difficult for any particular phase increment because the unusually high velocity gradient in microscale cavities was only accentuated by the presence of the oscillatory component. Additionally at specific frequencies, 13 Hz for example a significant phase lag was observed between flow in the cavity and flow in the freestream creating a shearing motion. Velocity fields were helpful in examining the pulsatile flow velocity profile in time for the flow approaching in the freestream however due to the large variation in flow velocities were difficult to scale onto a viewable plot within the cavity. To visualize time periodic flow in the cavity streamlines were calculated. These streamlines revealed the presence of circulations among other flow features at different increments of phase within the cavity which did not exist under steady conditions. Figure 2.19 shows two timesteps of the streamline images sequence at 80 Hz.

2.4.2.1 Influence of Wo and amplitude on pulsatile transport with Re = 1

The influence of pulsatile flow frequency was examined through the variation of the Wormersley numbers over a range of 0 to 1. At very low Reynolds numbers in the limit of stokes flow the input of an oscillatory component should superimpose linearly over the mean flow and the flow should remain reversible at all times. Therefore in this regime quantities such as residence times should

remain unaffected by the input of pulsation. However since the flows examined are not Stokes flows there is an inherent irreversibility which should be affected by the input of unsteadiness and hence the mixing properties of cavity ventilation. Examining the velocity fields for the pulsatile flow cases it is easy to see the oscillatory flow imposed on top of the mean flow provided by the syringe pump. A summary of these velocity fields can be found in Appendix F. Additionally since Wo are in the range of 0 to 1 the velocity profile remains roughly parabolic through all phase increments are predicted for pulsatile flow in a rigid system. The time averaged peak velocities as well as velocity profiles throughout two periods are also found in the Appendix F for all pulsatile flow cases.

2.4.2.2 Time averaged shear stress versus Wo

Time averaged shear was examined for the four frequency conditions spanning Womersley numbers as well as both amplitudes. Time averaged shear in the pulsatile cases was defined the same as the shear for the steady case except averages were taken along the top of the cavity for all phase increments. These spatial averages were then averaged in time to obtain the values plotted in Figure 2.20. Figure 2.20 show the time averaged shear for Womersley numbers of 0, 0.34, 0.84 and 1 as well as 1 under the reduced amplitude conditions. Although the amplitude did not remain constant throughout the range of frequencies the peak in shear does not correspond to the peak in flow amplitude. In all cases the affect of pulsation was to increase the time averaged shear experienced by the cavity. The mean flow in all cases was measured to be 30 mm/s +/- 1 mm/s. Suggesting that the data was not imaged in the direct center of the flow channel. The increase in time averaged shear was only 30 % relative to normal mean shear in the cavity under steady flow conditions at Re = 1. The uncertainty of the shear measurements is estimated to be on the order of 5%. The peak flow amplitude versus frequency decreases whereas the plot in Figure 2.20 suggests there is a peak within Wo 0 to 1. Fitting the data with a cubic spline we find an approximate Wo of 0.7 as the location of the peak as well as point to the existence of a resonant peak for time averaged shear across the top of the cavity under pulsatile flow conditions. As the Wo passes over the peak the shear begins to decrease, contrary to intuition, demonstrating that frequencies may exist in which time averaged shear at the top of the cavity could be equal to or less than the shear in steady flow conditions. The influence of amplitude on time averaged shear in the pulsatile cases was explored by examining two amplitudes corresponding to peak to peak of 80 mm/s and 5 mm/s. Although these peak to peak amplitudes differ by a factor of 16 and with 80 mm/s amplitude the flow reverses whereas at 5 mm/s peak to peak flow amplitude it does not the time averages shear stress values at the top of the cavity differ only by 5%.

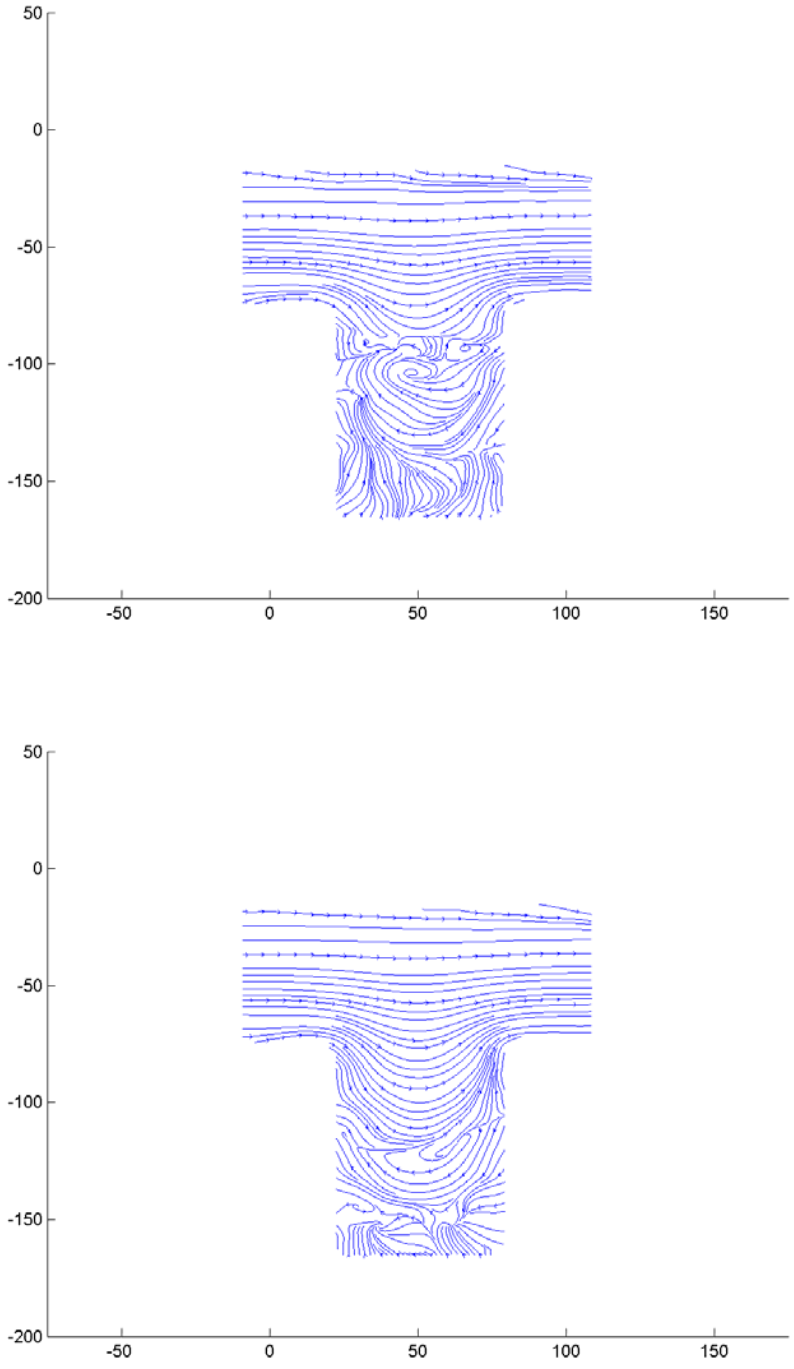

Figure 2.19: Two streamline images at phase time steps t = 0.00 seconds and t = 0.00125 seconds. These frames show the dynamic nature of the streamlines throughout time in the cavity.

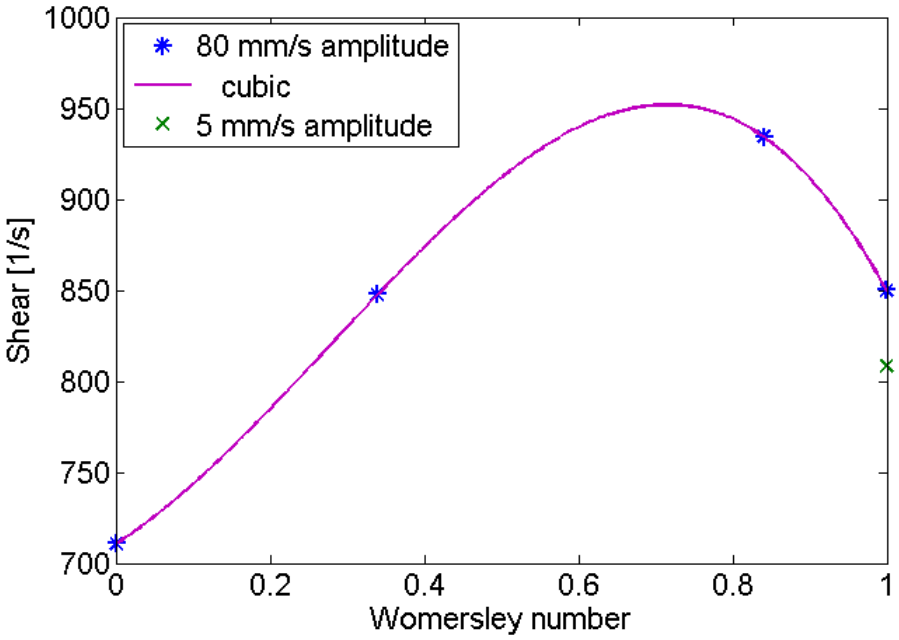

Figure 2.20: A plot of the pulsatile time averaged shear versus Womersley number for Wo = 0, 0.34, 0.84 and 1 for amplitudes of 0.4mm and 0.2 mm with respect to the voice coil probe displacement.

2.4.2.3 Residence times under pulsatile conditions

Residence time calculations were also performed for the pulsatile flow cases. In these cases the motion of the particles was largely dominated by the oscillatory component due to its relative size to the mean component locally inside of the cavity. The plot in Figure 2.21 shows the data points from the both the 0.4 mm amplitude and 0.2 mm amplitude trials. A rough cubic fit to the residence time calculation data also suggested the presence of a peak around Wo = 0.7 similar to the peak found in the average shear plot. Residence times were not normalized in this case due to the fact that the mean shear was approximately equal in all cases. The persistence of this apparent peak in two completely independent calculations suggests it is a real affect experienced by flow within the cavity opposed to just a strict increase in the residence time of particles versus the steady case as would be expected if for all times particles remained on the same streamlines. The affect of amplitude on the residence times of particles in the cavity was examined at a frequency of 113.14 Hz. Strangely but similar to the time averaged shear stress the amplitude had little to no distinguishable affect on the residence times and actually increased slightly.

2.4.2.4 Lagrangian coherent structures in pulsatile cavity flows

The FTLE fields for the pulsatile flow cases were able to define rough boundaries for the visualization of the fluid exchange occurring periodically through time within the cavity. Similar to the steady

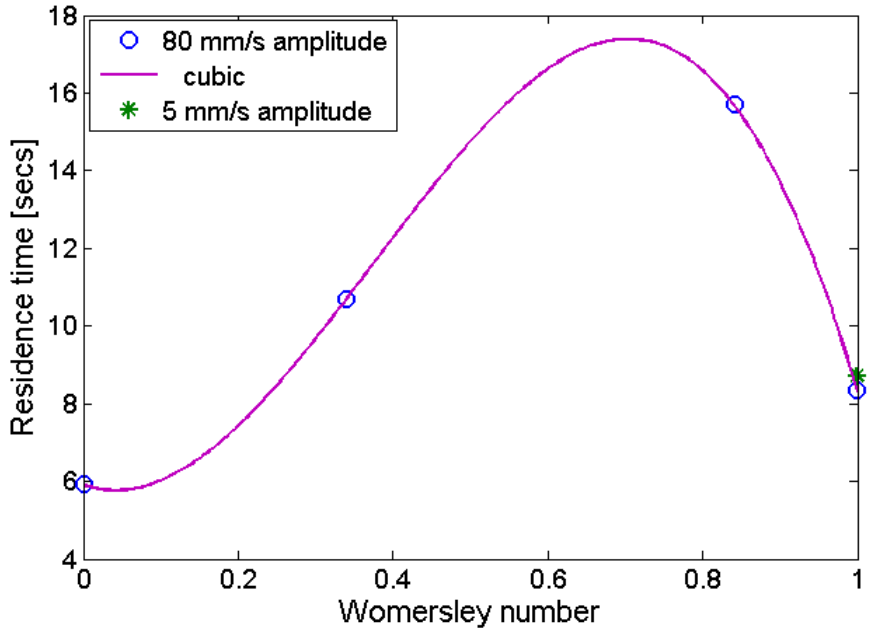

Figure 2.21: A plot of pulsatile residence times for different Wo numbers at amplitudes of 0.2 mm and 0.4 mm. The data suggests the possibility of a frequency dependent peak for the residence times of particles in the cavity. A spline fit to the data locates this peak at a Wo of approximately 0.7.

FTLE fields in portions of the phase where there is a large unidirectional flow the FTLE fields reveal LCS at the separation and reattachment at the top of the cavity for the backward time and forward time calculations respectively. At other increments within each period interesting flow structures were revealed that exist on millisecond timescales. Since the complete time series of FTLE fields is approximately 100 frames in length a few example overlays processed the same as was described for the steady case will be discussed. Also posing a difficulty was the large velocity gradient from the top of the cavity to the bottom making picking one integration time which clearly resolved structures into the lower reaches of the cavity but short enough to prevent particles near the top of the cavity from leaving the boundary. Figure 2.22 depicts the overlay of the forward time and backward time LCS at a frequency of 80 Hz. At t = 0.000375 sec the attracting or backward time LCS creates an attracting tentacle like structure which sweeps upward over the next 125 μsec. In the frame on the top of Figure 2.22, this tentacle along with the backward time LCS emerging from the trailing edge of the cavity enclose a packet of fluid which is squeezed between these two LCS structures during the next time step, shown in Figure 2.22 on the bottom. This tentacle also entrains particles from the base of the cavity promoting the expulsion of particles into the freestream. This behavior can be seen in the particle images in Figure 2.23. Notice how the influence of the pulsatililty is to distribute particles more evenly throughout the freestream depicted in part a) and b) in Figure 2.23. The entire motion of the LCS throughout the period is difficult to describe with only a few

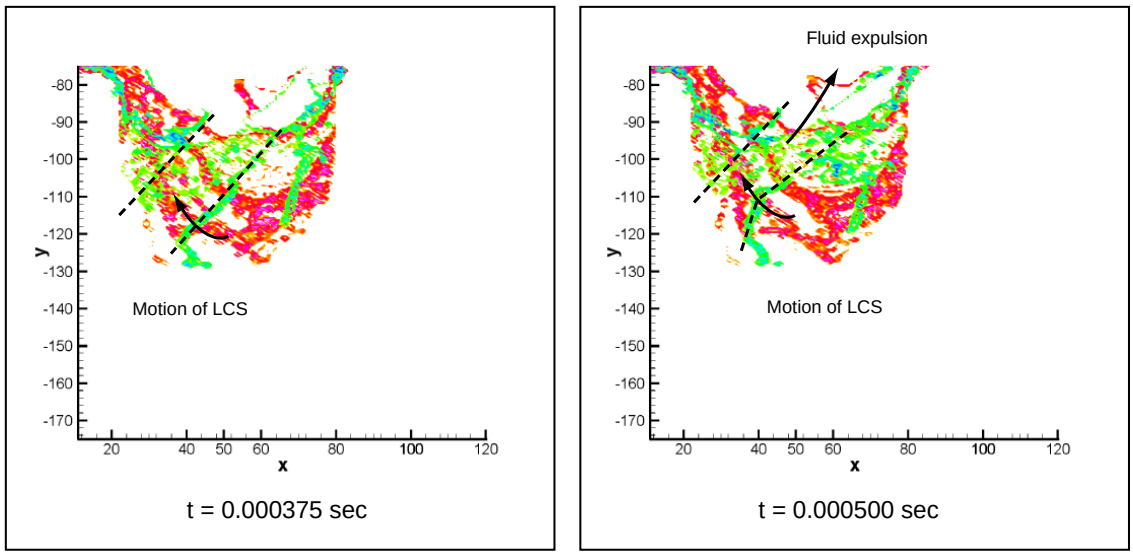

Figure 2.22: The forward and backward time LCS overlaid at two different time steps. On the left t = 0.000375 sec and on the right t = 0.000500 sec at 80 Hz.

frames, however these types of interactions between structures present within the cavity occur over multiples time steps in multiple phase increments throughout any given period and are prevalent in all pulsatile cases examined, 13 Hz, 80 Hz, and 113.14 Hz. Although far from identical to the 113.14 Hz large amplitude case with only 5 mm/s of pulsation amplitude the affect generally is to decrease the length to which tentacle like structures penetrate into the cavity and decrease the sharpness of the FTLE ridges and hence the LCS.

2.5 Conclusion

Microscale cavity flows were examined over a wide range of parameters for both steady and pulsatile flows. Transport was examined using both residence time calculations and Lagrangian Coherent Structures to reveal boundaries to transport within the flow. For steady cases the affects of cavity aspect ratio and mean freestream flow rate were examined for AR = 0.5, 1, 2 and mean freestream flow rates from 0.18 μL/min to 180 μL/min, equivalent to a Re range of 0.1 to 100. Pulsatile flows were examined at a mean freestream Re = 1 for a range for frequencies from DC to 113.14 Hz, equivalent to a Wo spanning 0 to 1.

1. Steady flow studies showed the stability of the separation in smaller aspect ratio cavities.

2. This stability was also represented in the penetration depth study where the the effective destablization of the separation by fluid entrainment is increased at higher aspect ratios meaning that higher Reynolds numbers are required for higher aspect ratio cavities to resist reat-

tachment to the cavity base as well as to minimize the penetration depth.

3. Time averaged shear stress in steady flow at the top of the cavity increases linearly with freestream Reynolds number.

4. In the steady cases ventilation into and out of the cavity reached a maximum slightly after the onset of recirculation pointing to a narrow region where the presence of a recirculation aids in the washout of particles from the cavity.

5. Contrary to the time averaged shear results in the steady case, pulsatile results of time averaged shear revealed a resonance for cavities under pulsatile flow forcing.

6. The residence time calculations in the pulsatile cases displayed a similar resonant peak pointing to some correlation between time averaged cavity shear and the inhibition of transport into or out of the cavity. The presence of this peak also points to the fact that there are frequencies which will have little or even a possibly negative affect on transport.

7. LCS calculations performed on the pulsatile flow studies revealed the presence of time periodic boundries emanating from the freestream and extending into the cavity depth. Their back and forth action periodically in time provides a qualitative mechanism for the expulsion of particles from the cavity and their distribution throughout the freestream.

This study show the affect of pulsation in microscale cavity flows can be both beneficial and detrimental to transport into and out of the cavity. Further investigation is desired to fully quantify the extent of mixing within the cavity under pulsatile flow conditions in particular emphasizing the affect of pulsation amplitude.

Microscale cavity flows are relevant to many flows on the microscale ranging from microfabrication to biofluid flows in grafts and stents. Here it has been demonstrated that a simple parameter such as the frequency of the flow can have a profound influence on the transport in microscale voids and cavities and in many cases the fluid mechanics of this relationship may determine the efficacy of the device in the case of a graft or stent or the throughput in the case of microfluidics. Although more detail is necessary before the parameter space is completely understood this work serves to illustrate some of the basic modes transport and serve as a starting point for understanding how pulsatile flows can be used to provide enhanced performance for applications such as thermal management, or sorting and filtration at the microscale.

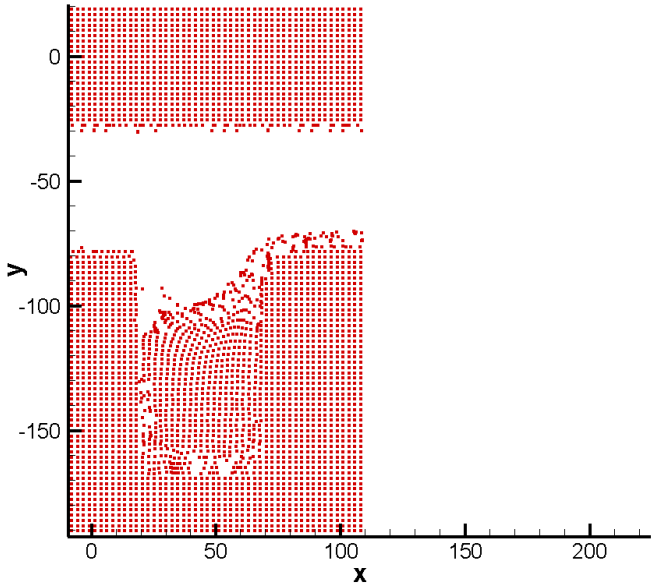

(a) A

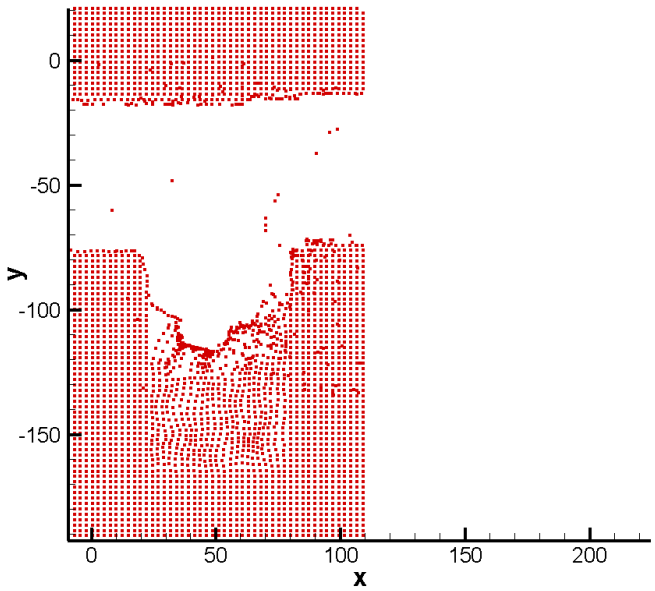

(b) B

Figure 2.23: The behavior of the ventilation process under a) steady and b) pulsatile conditions at 80 Hz. Note the tendency of particles remain near the wall in the steady case.